Tin-alloy heterostructures encapsulated in amorphous carbon nanotubes as hybrid anodes in rechargeable lithium ion batteries

Xifei Li[a], Yu Zhong[a], Mei Cai[b], Michael P. Balogh[b], Dongniu Wang[a], Yong Zhang[a], Ruying Li[a], Xueliang Sun[a,*]

[a] Department of Mechanical and Materials Engineering, University of Western Ontario, London, Ontario, N6A 5B9, Canada
[b] General Motors R&D Center, Warren, MI 48090-9055, USA

ARTICLE INFO

ABSTRACT

Sn anode in rechargeable lithium ion batteries (LIBs) is currently being intensely investigated due to high reversible capacity and energy density as compared to the commercialized graphite anode. However, large volume change upon cycling causes poor cyclic performance, which prevents the practical application of Sn anode in LIBs. In this study, the nanosized M_xSn (M = Ni, Fe, and Cr) alloys were encapsulated in amorphous carbon nanotubes (ACNTs) creating hybrid anode heterostructures. The structure of the hybrid anodes was confirmed by X-ray diffraction (XRD), field emission scanning electron microscope (FE-SEM) and high angle dark field scanning transmission electron microscope (HAADF-STEM), and demonstrated that Ni_3Sn_4, $FeSn_2$, and Cr_2Sn_3 alloys exist in the hybrid anodes as both nanowires and nanoparticles. The galvanostatic cycling originating from over 330 charge–discharge cycles indicated that encapsulation of Ni_3Sn_4, $FeSn_2$, and Cr_2Sn_3 into ACNTs results in surprisingly excellent cycling performance, high rate capability, and increased initial coulombic efficiency (81.4%). Ex situ HAADF-STEM images of anodes after cycles showed that one-dimensional ACNTs as well as electrochemically inactive phase M (Ni, Fe, and Cr) in M_xSn function as good matrices, offering "buffer zone" to effectively accommodate the mechanical stress induced by Sn anode expansion and shrinkage. Importantly, ACNTs enable electrical contact of Sn nanoparticles with the current collectors. Therefore, our design can significantly overcome electrochemical degradation of anodes with large volume change, resulting in increased LIB performance.

© 2012 Published by Elsevier Ltd.

1. Introduction

A transition from petroleum to an electrified automotive transportation system is a goal of utmost importance to society. Much effort and investment are being invested in accelerating the development of practical hybrid electric vehicles (HEVs) and plug-in hybrid electric vehicles (PHEVs) throughout the world [1]. A popular energy storage system, the rechargeable lithium ion battery (LIB), has been employed during the last two decades as an energy source for portable electronics. Moreover, it is still regarded as one of the most promising energy storage strategies for practical HEV and PHEV applications [2,3]. However, the graphite anode in a commercial LIB has a theoretical capacity of 372 mAh g^{-1} as a result of limited lithium storage sites within sp^2 carbon hexahedrons corresponding to the intercalation compound LiC_6 [4,5]. This limited capacity cannot completely satisfy the pressing requirements of high-performance LIBs for HEVs and PHEVs. It has been reported

that the total battery capacity can be enhanced by approximately 1.6 times if the specific capacity of the anode material can be simply increased up to 600 mAh g^{-1} [6–8]. Sn anode is capable of a high reversible capacity (approximately 994 mAh g^{-1} from $Li_{4.4}Sn$), being one of the most promising candidates to replace graphite anode for LIBs [9–12].

The high energy capacity of Sn anode results from different amounts of lithium insertion with a range of Li_xSn ($x \le 4.4$) alloys during discharge process. When a maximum amount of 4.4 lithium alloy with Sn to form $Li_{4.4}Sn$ (a 440% increase in the number of atoms), a large volume expansion (259%) inevitably occurs [13–15]. Conversely, a large volume contraction occurs during de-alloying process. Upon cycling, the repeated volume expansion and contraction cause considerable stress in Sn lattice, which results in cracking and crumbling of Sn anode. As a result, Sn anode crumbling causes a loss of electrical contact with the current collectors [16], thus poor cycle performance, prohibiting Sn anode application in high performance LIBs [17]. Recently, three important strategies have been addressed to circumvent these challenges: (1) nanosized Sn [18,19], (2) Sn based alloys [20–22], and (3) Sn-matrix composites [23–26]. Introducing a matrix into Sn anode can significantly

mitigate the large volume change problem and relieve mechanical stress in Sn lattice, thus enhancing anode performance [27–31]. Due to its good elasticity and high electrical conductivity, one-dimensional (1D) nanostructured carbon has been demonstrated as an excellent matrix, offering a "buffer zone" to accommodate the mechanical stress induced by the Sn anode's expansion and contraction [32,33,36]. Recently, Sn nanoparticle/single-walled carbon nanotube composites were reported to enhance anode durability (535 mAh g^{-1} in the 50th cycle at 0.2 C) [34]. Nanocrystalline Sn encapsulated in mesoporous carbon nanowires showed increased cycling performance with a reversible capacity of 710 mAh g^{-1} after 50 cycles at a current density of 100 mA g^{-1} [35]. Yu et al. encapsulated Sn@carbon nanoparticles in bamboo-like hollow carbon nanotubes (CNTs) and obtained a high reversible capacity of 737 mAh g^{-1} after 200 cycles at 0.5 C [36]. Obviously, nano-Sn encapsulated in a 1D nanostructured carbon matrix structure can effectively mitigate the volume change of Sn anode and improve cyclic stability. However, a further increase in Sn anode battery performance is still a significant challenge.

On one side, CNTs have been one of the most common 1D carbon materials because of various remarkable characteristics including outstanding electrical properties, high mechanical strength, high chemical stability, high aspect ratios, and a large activated surface area [37,38], making them a good matrix candidate for Sn anode with the large volume change problem. On the other side, it remains a great challenge to synthesize metallic Sn alloy nanostructures because relatively low melting point (232 °C) of Sn material makes high temperature fabrication of nanostructured Sn alloys difficult. Herein, we combined three important strategies together (nano-sized Sn, Sn based alloys, and Sn-matrix composites), and proposed a novel anode system – nanoscaled Sn alloys encapsulated in 1D CNTs to increase battery performance. In this study, the nano-Sn alloy composites with amorphous CNTs (NSAC-ACNTs) were for the first time proposed and demonstrated that their use as the hybrid anodes in LIBs can significantly improve cyclic performance and rate capability.

2. Experimental

2.1. Synthesis of hybrid anodes

NSAC-ACNTs were synthesized via a chemical vapor deposition (CVD). In a typical CVD procedure schematically illustrated in Fig. S1, the Sn powder precursor was loaded in a ceramic boat, which was then put in the center of a quartz tube furnace. The grade 304 stainless steel substrate, pre-treated with hydrochloric acid (HCl), was placed downstream of Sn powder in Ar flow used as a carrier gas. The furnace was then heated up to 880 °C for 2 h under a mixed atmosphere of Ar (200 sccm) and ethylene gas (C$_2$H$_4$, 2–10 sccm) before being switched off and slowly cooled down to room temperature [41].

2.2. Characterization of hybrid anodes

X-ray powder diffraction (XRD) patterns were collected on a Bruker D8 Discover Diffractometer using Co K$_\alpha$ radiation (λ = 0.178897 nm) at 40 kV and 100 mA. The NSAC-ACNT morphologies were observed in a field-emission scanning electron microscope (FESEM, Hitachi S-4800) and a high angle dark field scanning transmission electron microscope (HAADF-STEM, JEOL 2100F). Raman spectra were obtained at room temperature using a HORIBA Scientific LabRAM HR Raman spectrometer system equipped with an optical microscope and a 532.4 nm laser as the excitation radiation.
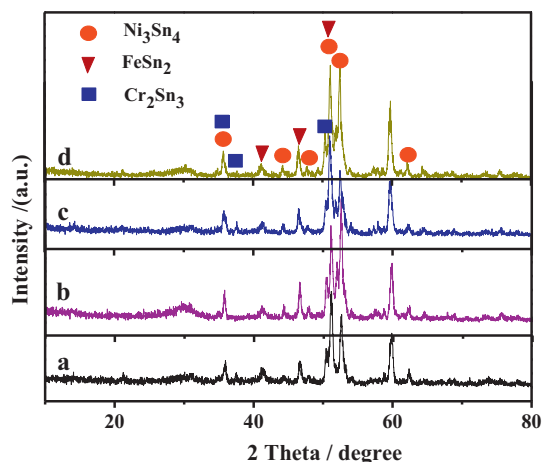

Fig. 1. XRD of NSAC–ACNT anodes after 0 cycle (a), 100 cycles (b), 200 cycles (c), and 330 cycles (d).

2.3. Electrochemical performance of hybrid anodes

CR-2325-type coin cells were assembled in a glove box under a dry argon atmosphere (moisture and oxygen level less than 1.0 ppm). After ultrasonic process was performed on the stainless steel substrate with deposited NSAC–ACNT, all deposited NSAC–ACNTs were scratched from the stainless steel, and were weighed to obtain the NSAC–ACNT weight. The specific capacities calculated were normalized by the NSAC–ACNT weight. The deposited NSAC–ACNT on the stainless steel with a diameter of 9/16 in. was used as a working electrode, a lithium foil as a counter electrode, and Celgard 2400 as a separator. The electrolyte was composed of 1.0 M LiPF$_6$ salt dissolved in ethylene carbonate (EC), diethyl carbonate (DEC), and ethyl methyl carbonate (EMC) in a 1:1:1 volume ratio. Cyclic voltammetry tests were performed on a versatile multichannel potentiostat 3/Z (VMP3) at a scan rate of 0.1 mV s^{-1} over a potential range of 0.01–3.0 V (vs. Li/Li$^+$). Charge–discharge characteristics were galvanostatically tested between 0.01 and 3.0 V (vs. Li/Li$^+$) at room temperature using an Arbin BT-2000 Battery Tester.

3. Results and discussion

In our previous report [39], core-shelled Sn@CNTs were successfully deposited on the carbon fiber of the carbon paper via a CVD process. But the carbon paper shows poor mechanical strength, providing some difficulties in LIB application. Herein, in this research, we study core-shelled Sn alloy@CNTs on a stainless steel as a novel anode in LIBs. The X-ray diffraction (XRD) was performed, and the characteristic XRD pattern of as-prepared NSAC–ACNTs is shown in Fig. 1a. A series of peaks can be clearly observed, but the peaks are different from the typical XRD pattern of the Sn phase, which results from some alloy formation at high temperature. The diffraction pattern in Fig. 1a exhibits obvious signals at 35.3°, 44.9°, 48.0°, 51.5°, 52.3°, and 62.5°, which are attributed to the characteristic peaks of Ni$_3$Sn$_4$ (JCPDS no. 4-845). Moreover, some diffraction peaks positioned at 41.0°, 45.8°, 51.5° match with FeSn$_2$ phase (JCPDS no. 73-2030). The Cr$_2$Sn$_3$ alloy can be also found as a result of several peaks of 35.3°, 38.5°, and 50.4° (JCPDS no. 19-333). There is a broad, weak peak centered at 30.9° to be observed due to the amorphous nature of CNTs [40]. Another peak at 59.8° is from the substrate. In order to further confirm the formation of Sn alloys, a elemental mapping was performed and shown in Fig. S2. Obviously, Sn, Fe, Ni, and Cr can be found to distribute along ACNTs, indicating the formation of M$_x$Sn alloys (M = Fe, Ni, Cr) encapsulated in ACNTs. As we
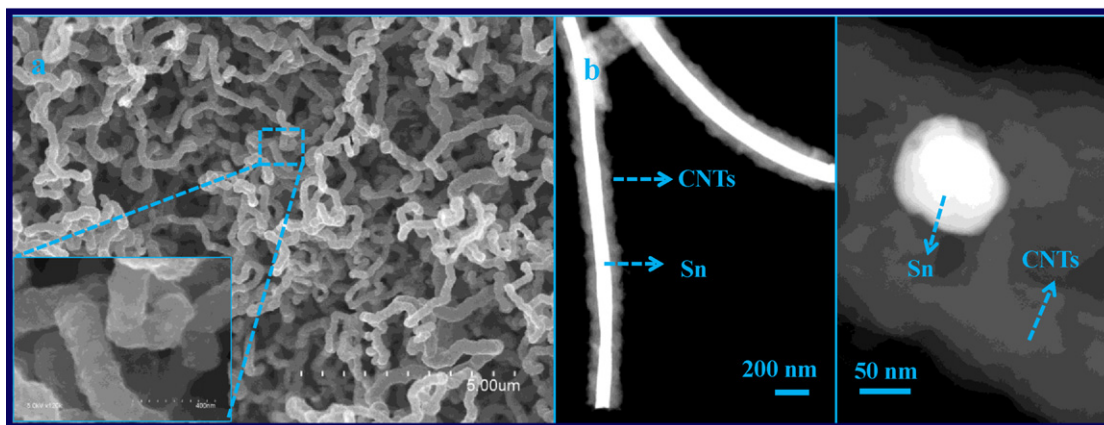
Fig. 2. (a) SEM and (b) HAADF-STEM images of NSAC–ACNT composite anodes.

previously reported [39,41], during thermal evaporation at 880 °C, Sn vapor is generated from the molten Sn powder (Sn with a melting point of 232 °C and a boiling point of 2270 °C). Sn vapor and the ethylene gas are transported downstream by the carrier gas. Sn as liquid droplets is deposited on the surface of the stainless steel substrate. A small amount of Fe, Ni, Cr from the stainless steel substrate can react with Sn to form the M_xSn alloys (M = Fe, Ni, Cr) as the initial nuclei which functions as catalyst to decompose the ethylene gas on the surface of the alloy droplets to produce CNTs. Furthermore, Sn vapor is continually absorbed at the top of the nuclei to promote the growth of the Sn alloy nanowire. The synchronous growth of CNTs and Sn alloy nanowire results in a hybrid NSAC–ACNT composite anode. In comparison to the most commonly used catalysts such as Fe, Co, Ni, the lower catalytic effectiveness of Sn might be responsible for the formation of amorphous CNTs rather than graphitic CNTs.

Fig. 2a shows FE-SEM images of as-prepared hybrid NSAC–ACNTs on the substrates obtained via CVD processing. A large number of NSAC–ACNTs with high density growth on the substrates is evident in the low magnification image shown in Fig. 2a. Entangled NSAC–ACNTs are uniformly grown on the substrate and show a flexual nanowire structure with a diameter of approximately 100–300 nm. Close examination reveals a rough surface on individual nanostructures (see the insert of Fig. 2a). HAADF-STEM examination Fig. 2b shows the typical morphology of nano-Sn alloys encapsulated in ACNTs. Scrutiny of nanostructured NSAC–ACNTs reveals two types of Sn alloy structures in Fig. 2b. One is an alloy nanowire core decorated by an ACNT shell, where the ACNT shell is ~60 nm thick and the diameter of the alloy nanowire core is ~110 nm. The other is an alloy nanoparticle with a diameter of ~100 nm encapsulated in ACNTs. Both structures as well as the alloy introduction can be beneficial to the Sn anode's performance because of the good matrix properties of ACNTs and the inative phase in the alloys.

Thermogravimetric analysis (TGA) was performed on hybrid SCNS–ACNTs obtained in an air flow at a heating rate of 10 °C min^{-1}. The obvious mass loss in the composites results from the oxidation of carbon nanotubes in air atmosphere (See Fig. S3). The mass increase above 750 °C is due to Sn oxidation into SnO_2 in air. The Sn content in the composite was estimated at 23.5 wt%. Similar Sn content was reported by several references to increase battery performance because high content matrix in the nanocomposites can effectively buffer large volume expansion/shrinkage of Sn anode [23,42–45].

NSAC–ACNT nanocomposite anode was initially examined by cyclic voltammetry (CV) at a scan rate of 0.1 mV s^{-1}, and the resulting cyclic voltammogram is shown in Fig. 3a. A cathodic peak centered at 0.72 V can be attributed to the formation of a solid electrolyte interphase (SEI) layer on the anodes. A weak peak at 0.36 V corresponds to the formation of lithiated phases [46,47]. The peaks corresponding to the formation of a series of Li_xSn alloys are not obvious because of the strong peak at ~0 V resulting from lithium intercalation into the ACNT shell. In the anodic scan, the peaks were observed at 0.60, 0.72, and 0.79 V and attributed to de-alloying of $Li_{4.4}Sn$ to form $Li_{2.33}Sn$, LiSn, and $Li_{0.4}Sn$ phases, respectively [47]. However, an abnormal peak positioned at ~2.93 V was also found in the first charge step, which is in agreement with other reports [48,49]. This peak existence originates from the presence of oxygen in the anodes and the fresh surface of the amorphous carbon [48,49].

Fig. 3b compares the first two voltage profiles of the NSAC–ACNT composite anode at a current density of 100 mA g^{-1}. NSAC–ACNT anode delivers a specific capacity of 350 and 285 mAh g^{-1} in the first discharge and charge, respectively. It has previously been reported that nanostructured Sn anode shows a low coulombic efficiency because of the large anode-electrolyte contact area, which results in the decomposition of the electrolyte to form an irreversible SEI layer on the anode surface [50–52]. The low coulombic efficiency of nanostructured anodes causes a sharp decrease in energy capacity for the practical LIBs, effectively preventing commercialization of nanosized Sn anode. Increasing coulombic efficiency of the nanoscaled anodes has long been a significant challenge [53]. In this research, nanosized Sn alloys are fully covered by the ACNT matrix, effectively decreasing the contact area between the nanoscaled anodes and the electrolyte, resulting in an increased coulombic efficiency. Consequently, the coulombic efficiency of NSAC–ACNT nanocomposites can reach 81.4% in the first cycle and increases to 91% in the second cycle; the second specific discharge and charge capacities reach 299 and 271 mAh g^{-1}, respectively. Furthermore, the coulombic efficiency approaches 100% in subsequent cycles (see Fig. 3c). However, in comparison to the theoretical capacity of Sn anode (994 mAh g^{-1}), obtained capacities from the composites are much lower as a result of the low content of Sn alloy as confirmed in Fig. S3. Future work will be done to increase this value to further enhance energy capacities.

The cycling performance at room temperature at a current density of 100 mA g^{-1} in a voltage range of 0.01–3.00 V is presented in Fig. 3c. Initially, there is a loss of capacity in the first 10 cycles – a 7% loss of the second capacity after 10 cycles – but as the cycling was continued from the 10th cycle up to the 233rd cycle, a significant gradual increase in the specific capacity was observed. The specific capacity reaches a maximum value (511 mAh g^{-1}) in the 233rd cycle and thereafter retains a good cyclability, decreasing only to 489 mAh g^{-1} in the 330th cycle. Clearly, our nanocomposite
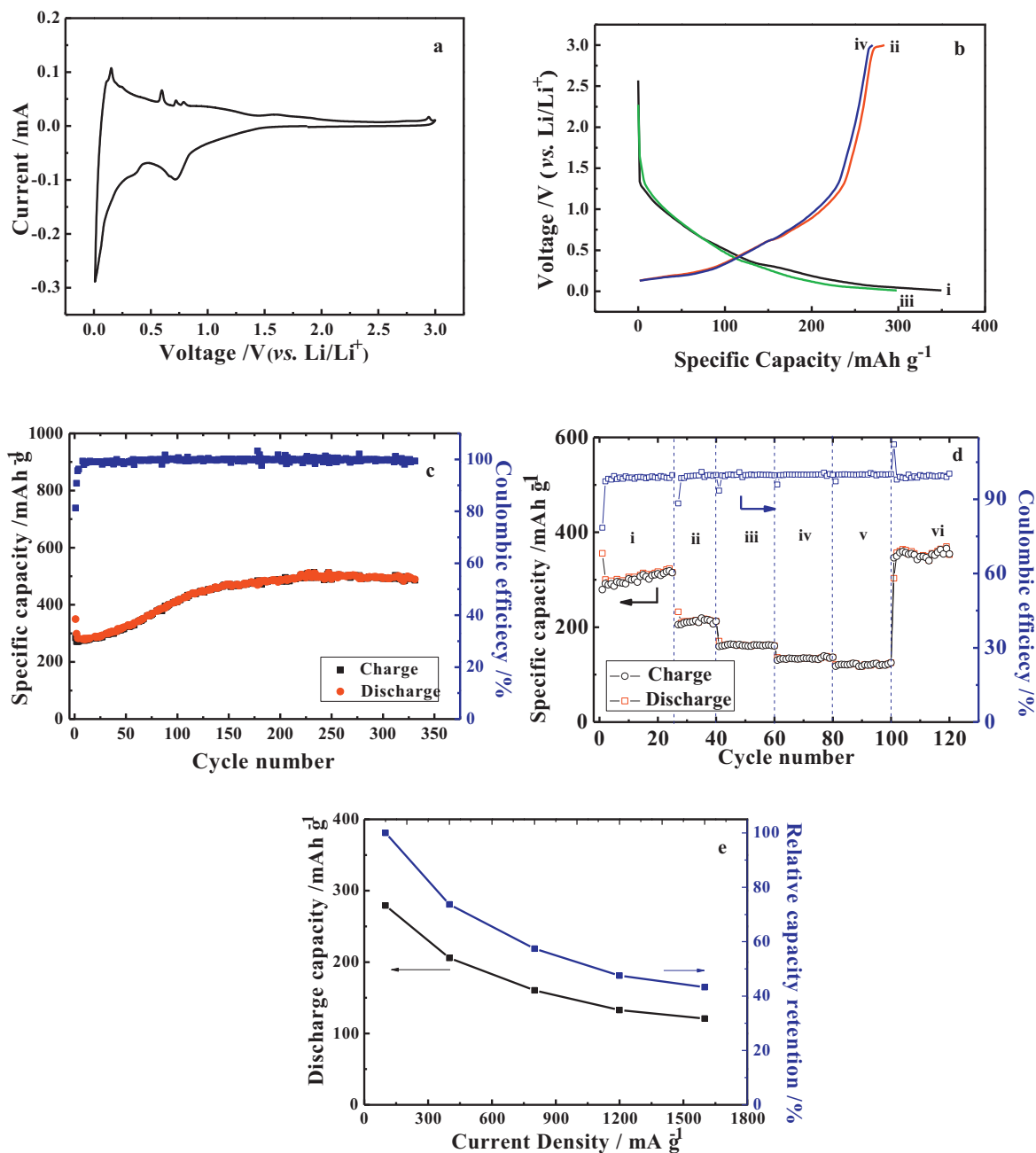
Fig. 3. (a) Cyclic voltammetry of NSAC–ACNT composite anodes at a scan rate of 0.1 mV s^{-1}; (b) charge/discharge profiles and (c) reversible charge/discharge capacity verse cycle numbers of NSAC–ACNT composite anode at a current density of 100 mA g^{-1} in a voltage range of 0.01–3.00 V at room temperature; (d) rate capability of NSAC–ACNTs at various current rates from 100 to 1600 mA g^{-1}: (i) 100, (ii) 400, (iii) 800, (iv) 1200, (v) 1600, and (vi) 100; (e) discharge capacity of NSAC–ACNTs as a function of current density from 100 to 1600 mA g^{-1}.

anodes possess a superior cycle performance in LIBs. As shown in the rate capability test in the region i–vi of Fig. 3d, NSAC–ACNT nanocomposites remain stable even at current densities as high as 1600 mA g^{-1}. Moreover, after undergoing 100 cycles at various current densities, a 101st cycle at a current density of 100 mA g^{-1} returned the cell to a higher reversible capacity than it had before at the same current density. Moreover, the retained discharge capacity of the hybrid anodes at various current densities was compared with that of a 100 mA g^{-1} current density, as shown in Fig. 3e; the hybrid anodes were found to sustain high capacity retention at current densities of 400, 800, 1200, and 1600 mA g^{-1}, relative to the capacity at 100 mA g^{-1}. On the other side, as shown in Fig. 3d, the hybrid anodes can still exhibit high coulombic efficiency when the current densities increase in a range of 100–1600 mA g^{-1}. The

results of the cycling performance and the rate capability indicate that introducing an ACNT matrix, as a physical buffer is an accessible and effective approach to improve the cyclability of Sn anode. ACNTs as well as the inactive Fe, Ni and Cr in Ni$_3$Sn$_4$, FeSn$_2$, and Cr$_2$Sn$_3$ alloys could provide strong matrices for nano-Sn, which alleviates problems with mechanical stresses resulting from large volume change that occurs during a charge–discharge cycle, and increases the structural stability of the Sn anode. As a result, NSAC–ACNTs greatly improve the cycling performance and the rate capability of Sn anode.

XRD, FE-SEM, and HAADF-STEM techniques were employed to discover why NSAC–ACNT hybrid nanocomposites show an improved cycle performance. The XRD patterns are shown in Fig. 1b–d. Of particular interest is that the XRD patterns of cycled
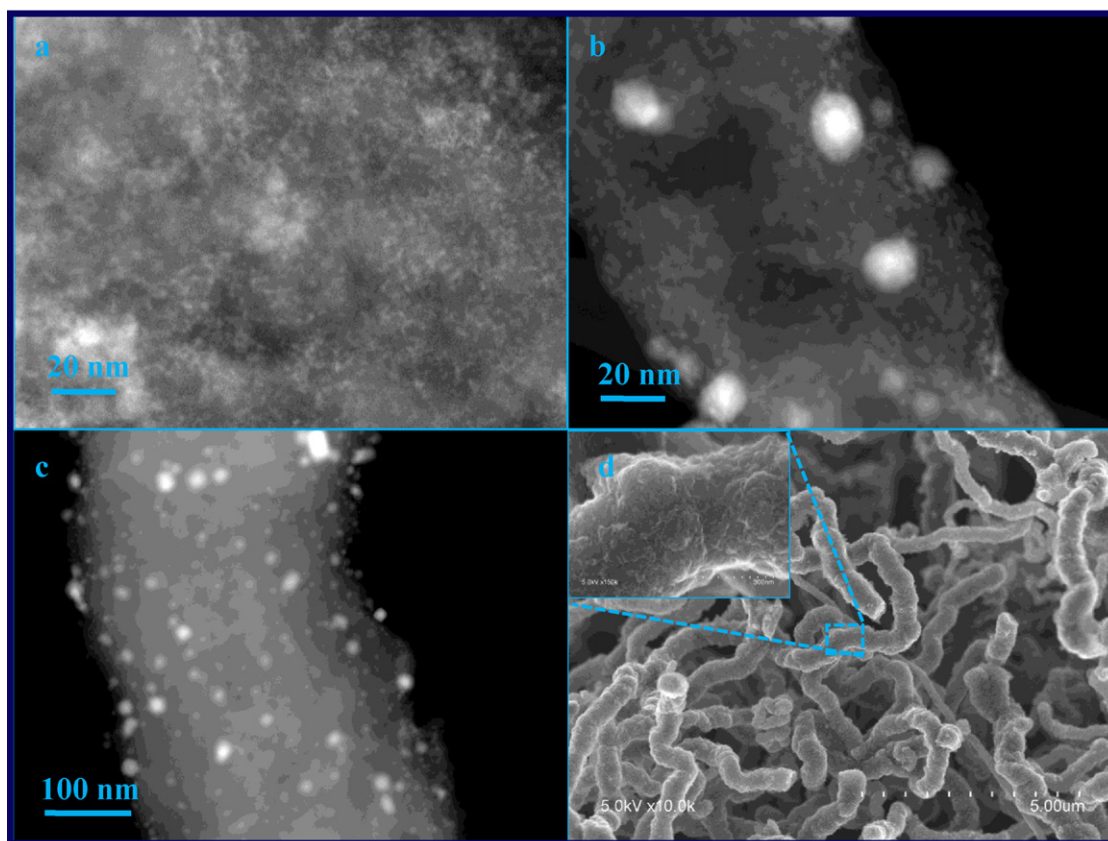
Fig. 4. Representative HAADF-STEM and SEM observation of NSAC–ACNT composite anodes after 100 cycles (a), 200 cycles (b), and 330 cycles (c and d).

electrodes are not appreciably different from that of the pristine electrode, suggesting a stable NSAC–ACNT hybrid nanocomposite structure upon cycling. Fig. 4 presents HAADF-STEM and FE-SEM images of Sn anode after 100, 200, and 330 charge–discharge cycles between 0.01 and 3.00 V at a current density of 100 mA g^{-1}. Compared to HAADF-STEM images of the initial nanocomposites in Fig. 2b, the hybird structures in Fig. 4a–c show obvious changes after repeated charge–discharge cycles. As shown in Fig. 2b, as-prepared nano-Sn alloys include two nanostructures such as nanowires and nanoparticles; after cycling, however, only nanoparticles are observed. Under the stresses caused by large charge–discharge volume change, it is possible that the alloy nanowires are pulverized into the nanoparticles. The nanoparticles found in Fig. 4a–c are in the 1–10 nm size range, much smaller than the pristine nanoparticles and nanowires; these nanoparticles with smaller size also increase the contact area with the electrolyte. These types of anode-electrolyte surface area increases would also explain the observed cell capacity increases with increased numbers of cycles [49]. But the existence of ACNTs can keep electrical contact of these nanoparticles with the current collectors. The FE-SEM image shown in Fig. 4d indicates that the electrode backbone remains intact and unchanged during electrochemical cycling except for a slight increase in diameter. The larger diameter is a result of large Sn lattice expansion/shrinkage upon cycling, highlighting the importance of ACNT matrix and the alloys in the stabilization of the cycling performance of nano-Sn anode.

During discharge process, as the aforementioned discussion, active Sn anode alloys with lithium to form Li$_{4.4}$Sn, resulting in a large Sn lattice volume expansion. An important concept was proposed to mitigate this problem that the electrochemically active phase is embedded in a nonelectrochemically active phase as a "buffer matrix" to compensate for the expansion of the reactants

[54–56]. In this study, nanosized Ni$_3$Sn$_4$, FeSn$_2$, and Cr$_2$Sn$_3$ were encapsulated in ACNTs by a CVD technique. The ACNT matrix on the surface of Sn alloys and the existence of the inactive Fe, Ni and Cr in the alloys can significantly buffer volume expansion/contraction of the anodes and suppress the electrical contact loss of the active nanoparticles with the current collector. 1D nanostructure is electrically connected to the metallic current collector, as a result, all 1D nanostructures are capable of contributing to the energy capacity [57]. Moreover, 1D anodes can form an interconnected nanoporous structure that exhibits direct 1D electronic pathways allowing for efficient charge transport and plays an important role in the path of the transportation of ions between the electrolytes and the active
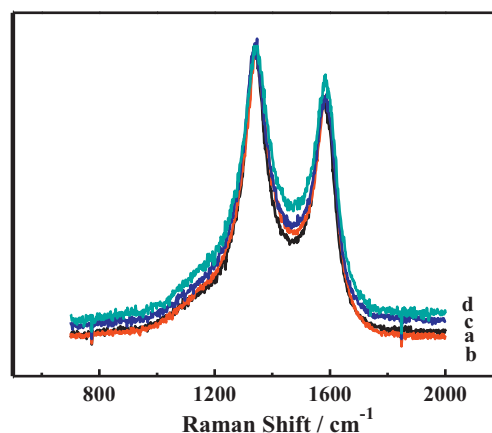
Fig. 5. Raman spectra comparison of NSAC–ACNT composite anode after 0 cycle (a), 100 cycles (b), 200 cycles (c), and 330 cycles (d).

materials [57]. Obviously, no binder is introduced in the proposed anode system. The absence of the binder can significantly increase electrical conductivity of the electrodes as well as energy density of the LIBs [58,59]. On the other side, the binder can initiate exothermic reactions and lead to potential explosions, and as a result, the binder-free anodes improve LIB abuse tolerance [60]. All of these benefits endow the proposed anode configuration with highly improved cycling performance and rate capability.

The evolution of the Raman spectra of NSAC–ACNTs with increasing charge–discharge cycles is shown in Fig. 5. When the number of cycles increases, the line width of the D band also increases. In the Raman spectra, the width of D band is used as an indicator of the in-plane structural ordering [61]. The D band line width increase indicates that ACNTs become less ordered and have defects with increasing charge–discharge cycles [62,63]. These defect sites also provide more electrochemically active locations and thus increase anode energy capacity [64–66].

4. Conclusions

In summary, we developed an effective CVD route to study NSAC–ACNT hybrid nanocomposites for LIB anodes. The ACNT matrix can effectively strengthen the low melting point encapsulated nano-Sn in a high-temperature growth process. As-prepared NSAC–ACNTs exhibit good cycling performance with up to more than 330 cycles and good rate capability with a higher current density of 1600 mA g^{-1}. The electrochemical stability improvement in the hybrid anode can be attributed to nanoscaled Ni_3Sn_4, $FeSn_2$, and Cr_2Sn_3 heterostructures encapsulated in ACNTs, which prevents aggregation and pulverization of nanosized Sn anode and increases the integration of the anodes during charge–discharge cycling application. Importantly, ACNTs keep electrical contact of Sn anode with the current collectors. Our finding discloses the influences of ACNT matrix and Sn-alloys on electrochemical performance of the anodes with high energy capacities as well as a rational direction to increase Sn-based anode performance in high performance rechargeable LIB applications.

Acknowledgements

Appendix A. Supplementary data

Supplementary data associated with this article can be found, in the online version, at http://dx.doi.org/10.1016/j.electacta.2012.11.097.

References

[1] G. Girishkumar, B. McCloskey, A.C. Luntz, S. Swanson, W. Wilcke, Lithium–air battery: promise and challenges, Journal of Physical Chemistry Letters 1 (2010) 2193.

[2] L.F. Cui, L.B. Hu, J.W. Choi, Y. Cui, Light-weight free-standing carbon nanotube-silicon films for anodes of lithium ion batteries, ACS Nano 4 (2010) 3671.

[3] L.W. Ji, X.W. Zhang, Evaluation of Si/carbon composite nanofiber-based insertion anodes for new-generation rechargeable lithium-ion batteries, Energy and Environmental Science 3 (2010) 124.

[4] D.Y. Pan, S. Wang, B. Zhao, M.H. Wu, H.J. Zhang, Y. Wang, Z. Jiao, Li storage properties of disordered graphene nanosheets, Chemistry of Materials 21 (2009) 3136.

[5] B.J. Landi, M.J. Ganter, C.D. Cress, R.A. DiLeo, R.P. Raffaelle, Carbon nanotubes for lithium ion batteries, Energy and Environmental Science 2 (2009) 638.

[6] X.F. Li, C.L. Wang, Engineering nanostructured anodes via electrostatic spray deposition for high performance lithium ion battery application, Journal of Materials Chemistry A 1 (2013) 165.

[7] M. Yoshio, T. Tsumura, N. Dimov, Electrochemical behaviors of silicon based anode material, Journal of Power Sources 146 (2005) 10.

[8] U. Kasavajjula, C.S. Wang, A.J. Appleby, Silicon anodes for Li-ion battery – a review, Journal of Power Sources 163 (2007) 1003.

[9] J. Yang, M. Winter, J.O. Besenhard, Small particle size multiphase Li-alloy anodes for lithium-ion batteries, Solid State Ionics 90 (1996) 281.

[10] I.A. Courtney, J.R. Dahn, Electrochemical and in situ X-ray diffraction studies of the reaction of lithium with tin oxide composites, Journal of the Electrochemical Society 144 (1997) 2045.

[11] A.H. Whitehead, J.M. Elliott, J.R. Owen, Nanostructured tin for use as a negative electrode material in Li-ion batteries, Journal of Power Sources 81/82 (1999) 33.

[12] G. Derrien, J. Hassoun, S. Panero, B. Scrosati, Nanostructured Sn–C composite as an advanced anode material in high-performance lithium-ion batteries, Advanced Materials 19 (2007) 2336.

[13] X.W. Lou, C.M. Li, L.A. Archer, Designed synthesis of coaxial SnO_2@carbon hollow nanospheres for highly reversible lithium storage, Advanced Materials 21 (2009) 2536.

[14] X.F. Li, C.L. Wang, Significantly increased cycling performance of novel "self-matrix" $NiSnO_3$ anode in lithium ion battery application, RSC Advances 2 (2012) 6150.

[15] X. Li, X. Meng, J. Liu, D. Geng, Y. Zhang, M. Banis, Y. Li, R. Li, X. Sun, M. Cai, M. Verbrugge, Tin oxide with controlled morphology and crystallinity by atomic layer deposition onto graphene nanosheets for enhanced lithium storage, Advanced Functional Materials 22 (2012) 1647.

[16] M.G. Kim, S. Sim, J. Cho, Novel core-shell Sn-Cu anodes for lithium rechargeable batteries prepared by a redox-transmetalation reaction, Advanced Materials 22 (2010) 5154.

[17] C. Liu, F. Li, L.P. Ma, H.M. Cheng, Advanced materials for energy storage, Advanced Materials 22 (2010) E28.

[18] T. Zhang, L.J. Fu, J. Gao, Y.P. Wu, R. Holze, H.Q. Wu, Nanosized tin anode prepared by laser-induced vapor deposition for lithium ion battery, Journal of Power Sources 174 (2007) 770.

[19] C.S. Wang, A.J. Appleby, F.E. Little, Electrochemical study on nano-Sn, $Li_{4.4}Sn$ and $AlSi_{0.1}$ powders used as secondary lithium battery anodes, Journal of Power Sources 93 (2001) 174.

[20] N.R. Shin, Y.M. Kang, M.S. Song, D.Y. Kim, H.S. Kwon, Effects of Cu substrate morphology and phase control on electrochemical performance of Sn–Ni alloys for Li-ion battery, Journal of Power Sources 186 (2009) 201.

[21] P.P. Ferguson, A.D.W. Todd, J.R. Dahn, Comparison of mechanically alloyed and sputtered tin–cobalt–carbon as an anode material for lithium-ion. batteries, Electrochemistry Communications 10 (2008) 25.

[22] S.H. Lee, M. Mathews, H. Toghiani, D.O. Wipf, C.U. Pittman, Fabrication of carbon-encapsulated mono- and bimetallic (Sn and Sn/Sb alloy) nanorods. potential lithium-ion battery anode materials, Chemistry of Materials 21 (2009) 2306.

[23] Y. Wang, J.Y. Lee, T.C. Deivaraj, Tin nanoparticle loaded graphite anodes for li-ion battery applications, Journal of the Electrochemical Society 151 (2004) A1804.

[24] K.D. Kepler, J.T. Vaughey, M.M. Thackeray, Copper–tin anodes for rechargeable lithium batteries: an example of the matrix effect in an intermetallic system, Journal of Power Sources 81 (1999) 383.

[25] M. Noh, Y. Kwon, H. Lee, J. Cho, Y. Kim, M.G. Kim, Amorphous carbon-coated tin anode material for lithium secondary battery, Chemistry of Materials 17 (2005) 1926.

[26] D. Deng, M.G. Kim, J.Y. Lee, J. Cho, Green energy storage materials: nano-structured TiO_2 and Sn-based anodes for lithium-ion batteries, Energy and Environmental Science 2 (2009) 818.

[27] A. Trifonova, T. Stankulov, M. Winter, Study of metal-supported carbon matrix as a high-capacity anode for Li-ion battery, Ionics 14 (2008) 421.

[28] Y. Wang, M.H. Wu, Z. Jiao, J.Y. Lee, Sn@CNT and Sn@C@CNT nanostructures for superior reversible lithium ion storage, Chemistry of Materials 21 (2009) 3210.

[29] X.F. Li, A. Dhanabalan, C.L. Wang, Three-dimensional porous core-shell Sn@carbon composite anodes for high-performance lithium-ion battery applications, Advanced Energy Materials 2 (2012) 238.

[30] M. Mouyane, J.M. Ruiz, M. Artus, S. Cassaignon, J.P. Jolivet, G. Caillon, C. Jordy, K. Driesen, J. Scoyer, L. Stievano, J. Olivier-Fourcade, J.C. Jumas, Carbothermal synthesis of Sn-based composites as negative electrode for lithium-ion batteries, Journal of Power Sources 196 (2011) 6863.

[31] R.Z. Hu, R. Liu, M.Q. Zeng, H. Wang, M. Zhu, Core/shell and multi-scale structures enhance the anode performance of a Sn–C–Ni composite thin film in a lithium ion battery, Journal of Materials Chemistry 21 (2011) 4629.

[32] S.J. Ding, J.S. Chen, X.W. Lou, CNTs@SnO_2@carbon coaxial nanocables with high mass fraction of SnO_2 for improved lithium storage, Chemisty: Asian Journal 6 (2011) 2278.

[33] S.J. Ding, J.S. Chen, X.W. Lou, One-dimensional hierarchical structures composed of novel metal oxide nanosheets on a carbon nanotube backbone and their lithium-storage properties, Advanced Functional Materials 21 (2011) 4120.

[34] J.H. Lee, B.S. Kong, S.B. Yang, H.T. Jung, Fabrication of single-walled carbon nanotube/tin nanoparticle composites by electrochemical reduction combined with vacuum filtration and hybrid co-filtration for high-performance lithium battery electrodes, Journal of Power Sources 194 (2009) 520.

[35] Y.C. Qiu, K.Y. Yan, S.H. Yang, Ultrafine tin nanocrystallites encapsulated in mesoporous carbon nanowires: scalable synthesis and excellent electrochemical properties for rechargeable lithium ion batteries, Chemical Communications 46 (2010) 8359.

[36] Y. Yu, L. Gu, C.L. Wang, A. Dhanabalan, P.A. van Aken, J. Maier, Encapsulation of Sn@carbon nanoparticles in bamboo-like hollow carbon nanofibers as an anode material in lithium-based batteries, Angewandte Chemie International Edition 48 (2009) 6485.

[37] K.P. Gong, F. Du, Z.H. Xia, M. Durstock, L.M. Dai, Nitrogen-doped carbon nanotube arrays with high electrocatalytic activity for oxygen reduction, Science 323 (2009) 760.

[38] X.F. Li, J.L. Yang, Y.H. Hu, J.J. Wang, Y.L. Li, M. Cai, R.Y. Li, X.L. Sun, Novel approach toward a binder-free and current collector-free anode configuration: highly flexible nanoporous carbon nanotube electrodes with strong mechanical strength harvesting improved lithium storage, Journal of Materials Chemistry 22 (2012) 18847.

[39] R. Li, X. Sun, X. Zhou, M. Cai, X. Sun, Aligned heterostructures of single-crystalline tin nanowires encapsulated in amorphous carbon nanotubes, Journal of Physical Chemistry C 111 (2007) 9130.

[40] H.C. Shin, M.L. Liu, Three-dimensional porous copper–tin alloy electrodes for rechargeable lithium batteries, Advanced Functional Materials 15 (2005) 582.

[41] Y. Zhong, Y., Zhang, R. Y. Li, X. L. Sun, submitted for publication.

[42] D. Deng, J.Y. Lee, Reversible storage of lithium in a rambutan-like tin-carbon electrode, Angewandte Chemie International Edition 48 (2009) 1660.

[43] K.T. Lee, Y.S. Jung, S.M. Oh, Synthesis of tin-encapsulated spherical hollow carbon for anode material in lithium secondary batteries, Journal of the American Chemical Society 125 (2003) 5652.

[44] Y. Liu, J.Y. Xie, Y. Takeda, J. Yang, Advanced Sn/C composite anodes for lithium ion batteries, Journal of Applied Electrochemistry 32 (2002) 687.

[45] Y.S. Jung, K.T. Lee, J.H. Ryu, D.M. Im, S.M. Oh, Sn-carbon core-shell powder for anode in lithium secondary batteries, Journal of the Electrochemical Society 152 (2005) A1452.

[46] M. Winter, J.O. Besenhard, Electrochemical lithiation of tin and tin-based intermetallics and composites, Electrochimica Acta 45 (1999) 31.

[47] M. Marcinek, L.J. Hardwick, T.J. Richardson, X. Song, R. Kostecki, Microwave plasma chemical vapor deposition of nano-structured Sn/C composite thin-film anodes for Li-ion batteries, Journal of Power Sources 173 (2007) 965.

[48] C.D. Gu, Y.J. Mai, J.P. Zhou, Y.H. You, J.P. Tu, Non-aqueous electrodeposition of porous tin-based film as an anode for lithium-ion battery, Journal of Power Sources 214 (2012) 200.

[49] S.Z. Liang, X.F. Zhu, P.C. Lian, W.S. Yang, H.H. Wang, Superior cycle performance of Sn@C/graphene nanocomposite as an anode material for lithium-ion batteries, Journal of Solid State Chemistry 184 (2011) 1400.

[50] G.X. Wang, B. Wang, X.L. Wang, J. Park, S.X. Dou, H. Ahn, K. Kim, Sn/graphene nanocomposite with 3D architecture for enhanced reversible lithium storage in lithium ion batteries, Journal of Materials Chemistry 19 (2009) 8378.

[51] X.W. Lou, J.S. Chen, P. Chen, L.A. Archer, One-pot synthesis of carbon-coated SnO_2 nanocolloids with improved reversible lithium storage properties, Chemistry of Materials 21 (2009) 2868.

[52] X.J. Zhu, Z.P. Guo, P. Zhang, G.D. Du, C.K. Poh, Z.X. Chen, S. Li, H.K. Liu, Three-dimensional reticular tin–manganese oxide composite anode materials for lithium ion batteries, Electrochimica Acta 55 (2010) 4982.

[53] B.K. Guo, J. Shu, K. Tang, Y. Bai, Z.X. Wang, L.Q. Chen, Nano-Sn/hard carbon composite anode material with high-initial coulombic efficiency, Journal of Power Sources 177 (2008) 205.

[54] Q.F. Dong, C.Z. Wu, M.G. Jin, Z.C. Huang, M.S. Zheng, J.K. You, Z.G. Lin, Superior cycle performance of Sn@C/graphene nanocomposite as an anode material for lithium-ion batteries, Solid State Ionics 167 (2004) 49.

[55] J. Hassoun, S. Panero, B. Scrosati, Electrodeposited Ni–Sn intermetallic electrodes for advanced lithium ion batteries, Journal of Power Sources 160 (2006) 1336.

[56] J.T. Yin, M. Wada, S. Yoshida, K. Ishihara, S. Tanase, T. Sakai, New Ag–Sn alloy anode materials for lithium-ion batteries, Journal of the Electrochemical Society 150 (2003) A1129.

[57] C.K. Chan, H. Peng, G. Liu, K. McIlwrath, X.F. Zhang, R.A. Huggins, Y. Cui, High-performance lithium battery anodes using silicon nanowires, Nature Nanotechnology 3 (2008) 31.

[58] S. Luo, K. Wang, J.P. Wang, K.L. Jiang, Q.Q. Li, S.S. Fan, Binder-free $LiCoO_2$/carbon nanotube cathodes for high-performance lithium ion batteries, Advanced Materials 24 (2012) 2294.

[59] X. Qin, X.H. Wang, J. Xie, L. Wen, Hierarchically porous and conductive $LiFePO_4$ bulk electrode: binder-free and ultrahigh volumetric capacity Li-ion cathode, Journal of Materials Chemistry 21 (2011) 12444.

[60] S.S. Zhang, T.R. Jow, Study of poly(acrylonitrile-methyl methacrylate) as binder for graphite anode and $LiMn_2O_4$ cathode of Li-ion batteries, Journal of Power Sources 109 (2002) 422.

[61] J.M. Vallerot, X. Bourrat, A. Mouchon, G. Chollon, Quantitative structural and textural assessment of laminar pyrocarbons through Raman spectroscopy, electron diffraction and few other techniques, Carbon 44 (2006) 1833.

[62] Y. Wang, D.C. Alsmeyer, R.L. McCreery, Raman spectroscopy of carbon materials: Structural basis of observed spectra, Chemistry of Materials 2 (1990) 557.

[63] J. Jehlicka, O. Urban, J. Pokorny, Raman spectroscopy of carbon and solid bitumens in sedimentary and metamorphic rocks, Spectrochimica Acta Part A 59 (2003) 2341.

[64] X.F. Li, J. Liu, Y. Zhang, Y.L. Li, H. Liu, X.B. Meng, J.L. Yang, D.S. Geng, D.N. Wang, R.Y. Li, X.L. Sun, High concentration nitrogen doped carbon nanotube anodes with superior Li$^+$ storage performance for lithium rechargeable battery application, Journal of Power Sources 197 (2012) 238.

[65] M. Winter, J.O. Besenhard, M.E. Spahr, P. Novak, Insertion electrode materials for rechargeable lithium batteries, Advanced Materials 101 (1998) 725.

[66] X.F. Li, D.S. Geng, Y. Zhang, X.B. Meng, R.Y. Li, X.L. Sun, Superior cycle stability of nitrogen-doped graphene nanosheets as anodes for lithium ion batteries, Electrochemistry Communications 13 (2011) 822.